Convergent Results from Experimental and Theoretical DFT Studies of the Intramolecular Rearrangement of *Z*-Hydrazones of 3-Acyl-1,2,4-Oxadiazoles†

Andrea Bottoni,*,‡ Vincenzo Frenna,§ Camilla Zaira Lanza,*,|| Gabriella Macaluso,§ and Domenico Spinelli||

Dipartimento di Chimica "G. Ciamician", via Selmi 2, 40126 Bologna; Dipartimento di Chimica Organica "E. Paternò", Viale delle Scienze, Parco d'Orleans 2, 90128 Palermo; and Dipartimento di Chimica Organica "A. Mangini", via S.Donato 15, 40127 Bologna

Received: August 12, 2003; In Final Form: December 2, 2003

A combined kinetic and theoretical study of the monocyclic rearrangements of heterocycles (MRH) has been carried out. The interconversion of the *Z*-hydrazone of 3-benzoyl-5-phenyl-1,2,4-oxadiazole into the corresponding triazole has been experimentally investigated in dioxane/water in the pS^+ range $5.5_5-13.9$. The uncatalyzed region has been examined at the DFT level using a model system formed by the *Z*-hydrazone of 3-formyl-1,2,4-oxadiazole and one or two water molecules. The environmental effect of the solvent has been emulated using a continuum model (COSMO) approach. The kinetic data suggest a concerted process where the magnitude of the activation barrier is determined by the interplay of two opposite factors, that is, the nucleophilicity of the nitrogen atom and the acidity of the nitrogen-bonded protons. The computations indicate the existence of two multistep reaction pathways. When the solvent environment is taken into account, the preferred path, which involves two water molecules acting as a base, becomes a concerted highly asynchronous path, where the nucleophilic attack and the proton transfer occur not simultaneously but in the same kinetic step.

Introduction

In the framework of their fundamental work on the heterocycle reactivity, Katritzky and Boulton pointed out the occurrence of two different classes of ring-to-ring interconversion of azoles: the "monocyclic rearrangements of heterocycles" (MRH) and the "bicyclic rearrangements of heterocycles" (BRH) (see Scheme 1).[1]

The BRHs have been widely investigated both at the experimental[1,2] and theoretical[3] level and a large number of papers are now available in the literature. Kinetic and thermodynamic studies have enlightened the influence of the substituents in the benzocondensed ring[1c−e] while, more recently, ab initio calculations have been used to foresee new possible bicyclic rearrangements.[3d]

The MRH processes are of much more general synthetic interest, since they disclose the way to several five-membered heteroaromatics[1a,c,4a−d] and dihydroheteroaromatics.[4e] These reactions, which do not require π-reorganization and only involve the formation and breaking of σ bonds,[1c,4c,d] have been the subject of several synthetic and mechanistic studies. Our group[4c−d,5] as well as other research groups (Harsanyi,[6] Katritzky,[1a−d] and Korbonits[4e,7]) have been working for a long time on this subject. Several new MRH examples have been discovered and their mechanism has been deeply investigated. In a series of papers,[4c−d,5a−d] we have quantitatively examined the ring-to-ring interconversion of many derivatives of 1,2,4-oxadiazole. We have compared the effects of different side chains linked at C−3 (X═Y−ZH = C═N−NH−Ar,[5a−d] NH−CO−NH−Ar,[8] N═CH−NH−Ar,[9] NH−CO−R),[10a−f] and we have carried out the reactions in various solvents (dioxane/water, dioxane, ethyl acetate, methanol, benzene, and acetonitrile) in the presence of different bases. The large sets of data collected in dioxane/water[4c,d,5a,b,8,9a] in the presence of buffers have provided kinetic evidence for the occurrence of two different kinds of reaction channels: a proton-concentration-independent pathway (*uncatalyzed pathway*)[11] and a proton-concentration-dependent one (*base-catalyzed pathway*, requiring either general or specific base catalysis). Moreover, we have recently pointed out the occurrence of a specific *acid-catalyzed pathway* for substrates **1** (see Scheme 1) when a basic center is present in the A═B segment.[5b] Also, data on isoxazoles[12a−b] and 1,2,5-

SCHEME 1

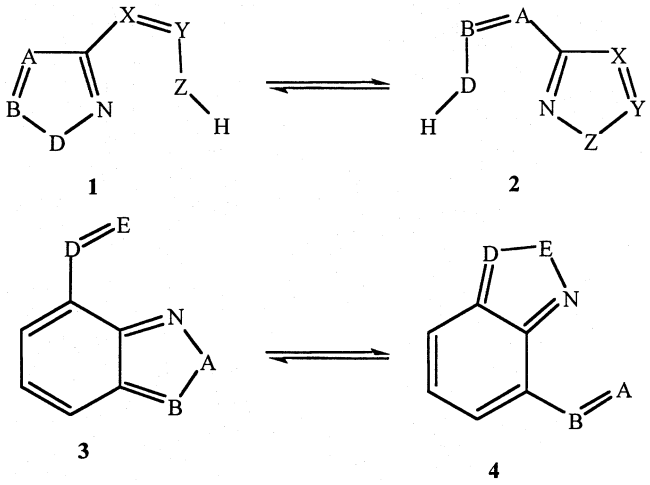

† Dedicated to Professor Alan R. Katritzky on the occasion of his 75th birthday.

* Address correspondence to these authors. E-mail: andrea@ciamserv.ciam.unibo.it.

‡ G. Ciamician.

§ E. Paternò.

|| A. Mangini.

10.1021/jp0309668 CCC: $27.50
Published on Web 02/13/2004

SCHEME 2

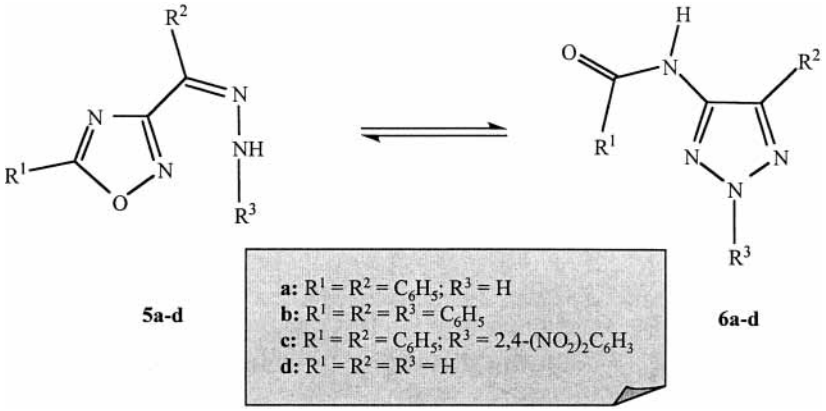

oxadiazoles[1a,b,4c,d,12c,d] have been collected to rationalize how the nature of the starting ring affects the reaction. The whole of the results obtained has evidenced that MRHs occur as intramolecular nucleophilic substitutions (S_{Ni}) and thus represent a special case of S_N2 displacement.

Notwithstanding its synthetic and mechanistic importance, the MHR has attracted only limited attention from a computational point of view. Semiempirical and ab initio calculations have provided information in the fully degenerate rearrangement of the anions of some acylamino derivative of isoxazole, 1,2,4- and 1,2,5-oxadiazole, which represents the most simple system that can be studied.[10c,e,g] Furthermore, the reactivity in the rearrangement of some 3-(2-aminoethyl)- and 3-(2-aminoaryl)-1,2,4-oxadiazoles has been correlated to CNDO/2 net charges on the N(2) atom.[7b] All these results are often characterized by an unsatisfactory agreement with experimental data.

In this paper, we report the results of a combined experimental and theoretical study of the MRH process. The kinetics of the conversion of the *Z*-hydrazone of 3-benzoyl-5-phenyl-1,2,4-oxadiazole (**5a** in Scheme 2) into the 1,2,3-triazole (**6a**) in dioxane/water is investigated in a large range of pS^+.[13a] The results are compared to previous data obtained for the *Z*-phenylhydrazone (**5b**)[13b] and the *Z*-2,4-dinitrophenylhydrazone (**5c**)[5a] to rationalize the effect of structural modifications in the X=Y−ZH side-chain. To obtain a better insight into the mechanistic details of this reaction, the rearrangement of the *Z*-hydrazone (**5d**) of 3-formyl-1,2,4-oxadiazole into the corresponding triazole (**6d**) is investigated at the DFT level. The model system used here emulates the reaction in the uncatalyzed region and includes one or two water molecules to describe the direct involvement of the solvent as a base.

Results and Discussion

A. Kinetic Study of the Rearrangement of 5a into 6a. The title rearrangement has been studied in dioxane/water (1:1, v:v) in the presence of buffers in the $5.5_5-13.9$ pS^+ range.[14] The apparent first-order rate constants for the rearrangement of **5a** [$(k_{A,R})_{5a}$] are collected in Table 1 and are reported in Figure 1 together with data concerning the ring-to-ring interconversion of **5b** and **5c**.

The examination of Figure 1 shows the expected influence of the proton concentration on the reactivity of **5a**. In the pS^+ range $5.5_5-9.0$ no change with pS^+ is evidenced (uncatalyzed pathway), while at $pS^+ > 10$ the reactivity increases with pS^+ (base-catalyzed pathway). Notwithstanding the high pS^+ values investigated (up to pS^+ 13.9), no limiting rate constant has been observed, suggesting for the base-catalyzed reaction the formation of a van't Hoff complex.[15a−b] The existence of an Arrhenius complex can be ruled out on the basis of the very low acidity of the $-NH_2$ protons of the hydrazone moiety. However, the *Z*-phenylhydrazone (**5b**)[13b] and the *Z*-2,4-dinitrophenylhydrazone

TABLE 1: Calculated Apparent Kinetic Constants (at 293 K) and Activation Parameters for the Rearrangement of 5a into 6a at Various pS^+ in Dioxane/Water

pS^{+a}	5.55	5.90	6.35	7.20	7.85	8.40
$10^8(k_{A,R})^b$	4.94	5.02	5.00	4.98	5.14	5.02
$\Delta H^{\#c}$	25.3	25.2	25.2	25.2	25.0	25.1
$\Delta S^{\#d}$	−5.6	−6.0	−5.8	−5.9	−6.6	−6.1
pS^{+e}	9.42	9.72	9.89	10.22	10.41	10.84
$10^7(k_{A,R})^b$	0.540	0.590	0.675	0.908	1.18	2.47
$\Delta H^{\#c}$	25.1	25.1	25.0	24.3	24.2	24.0
$\Delta S^{\#d}$	−6.1	−5.9	−6.0	−7.7	−7.6	−7.0
pS^{+e}	11.00	11.13	11.37	11.50	11.61	11.77
$10^7(k_{A,R})^b$	3.08	4.25	6.61	9.12	11.2	16.6
$\Delta H^{\#c}$	24.2	24.5	24.7	24.5	24.7	24.4
$\Delta S^{\#d}$	−5.7	−4.3	−2.4	−2.6	−1.4	−1.7
pS^{+e}	12.00	12.21	12.44	12.85	13.20	13.52
$10^5(k_{A,R})^b$	0.269	0.415	0.675	1.67	3.61	7.50
$\Delta H^{\#c}$	23.9	24.3	24.2	24.1	23.5	23.1
$\Delta S^{\#d}$	−2.3	+0.1	+0.4	+1.9	+1.1	+1.5
pS^{+e}	13.90					
$10^5(k_{A,R})^b$	16.6					
$\Delta H^{\#c}$	23.0					
$\Delta S^{\#d}$	+2.5					

[a] Citrate buffer; total buffer concentration 0.0125 M. [b] The unit is s^{-1}. Values calculated by activation parameters at 293 K; the experimental rate constants were measured in the range 293−333 K and were reproducible within ±3%. [c] The unit is kcal mol^{-1}. At 313 K the maximum error is 0.7 kcal mol^{-1}. [d] The unit is cal K^{-1} mol^{-1}. At 313 K the maximum error is 2 cal K^{-1} mol^{-1}. [e] Borate buffer; total buffer concentration 0.0125 M.

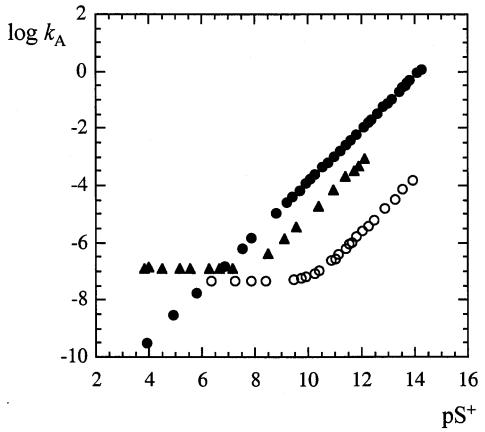

Figure 1. Plot of log k_A for the rearrangement of **5a** (○), **5b** (▲), and **5c** (●) into **6a**, **6b,** and **6c**, respectively, in dioxane/water at 293.15 K versus pS^+.

TABLE 2: Calculated Apparent Kinetic Constants (at 298 K) and Activation Parameters for the Rearrangement of 5a into 6a at Various pS^+ and Borate Buffer Concentrations in Dioxane/Water

pS^{+a}	10.84	11.00	11.13	11.37	11.50	11.61
$10^4(k_{A,R})^b$	0.501	0.708	0.873	1.37	1.88	2.32
pS^{+a}	11.77	12.00	12.21	12.44		
$10^4(k_{A,R})^b$	3.41	5.48	8.51	13.8		
pS^{+c}	10.95	11.05	11.18	11.44	11.64	11.85
$10^4(k_{A,R})^b$	0.706	0.860	1.14	1.89	2.88	4.41
$\Delta H^{\#d}$	24.3	23.9	24.0	24.2	23.9	24.0
$\Delta S^{\#e}$	−5.3	−6.2	−5.0	−3.7	−3.7	−2.6
pS^{+c}	12.00	12.17	12.52			
$10^4(k_{A,R})^b$	5.90	8.48	17.1			
$\Delta H^{\#d}$	24.2	23.5	23.9			
$\Delta S^{\#e}$	−0.9	−2.9	−0.3			
pS^{+f}	10.85	11.05	11.27	11.42	11.74	11.98
$10^4(k_{A,R})^b$	0.751	1.09	1.67	2.22	4.06	6.45
$\Delta H^{\#d}$	23.9	24.1	24.0	23.8	24.0	24.0
$\Delta S^{\#e}$	−6.5	−5.0	−4.7	−4.7	−2.7	−1.7
pS^{+f}	12.10	12.48				
$10^4(k_{A,R})^b$	8.09	16.6				
$\Delta H^{\#d}$	23.6	23.2				
$\Delta S^{\#e}$	−2.6	−2.7				

[a] Total buffer concentration 0.0125 M. [b] The unit is s^{-1}. Values calculated by activation parameters; the experimental rate constants were measured in the range 313−333 K and were reproducible within ±3%. [c] Total buffer concentration 0.0250 M. [d] The unit is kcal mol^{-1}. At 313 K the maximum error is 0.7 kcal mol^{-1}. [e] The unit is cal K^{-1} mol^{-1}. At 313 K the maximum error is 2 cal K^{-1} mol^{-1}. [f] Total buffer concentration 0.0500 M.

(**5c**),[5a] which both have a much more acidic (NH) proton, also show a similar behavior. To confirm this outcome, we have studied the rearrangement of **5a** in the pS^+ range 10.8−12.5 at different sodium borate−boric acid buffer concentrations (data in Table 2), observing a $(k_{A,R})_{\mathbf{5a}}$ increase with buffer concentration.[15c] A fitting of kinetic data to eq 1,[15,16] which represents the most general form for a base-catalyzed reaction, gives the results collected in Table 3. The statistical data give uncertain indication for the occurrence of the uncatalyzed pathway (k_u, being the small intercept of a multiparameter equation, should be more correctly obtained by direct measurement in the 5.5_5−9.0 pS^+ range). Also, these data indicate the absence of a significant contribution of k_A, $k_{A,B}$, or $k_{B,OH}$. These results point out the occurrence of two simple (bimolecular) general base-catalyzed pathways (at 298.15 K, k_{OH} 1.7×10^{-2} and k_B 4.2×10^{-5} l mol^{-1} s^{-1}, respectively) and definitively support the formation of a van't Hoff complex.

$$(k_{A,R}) = k_u + k_{OH}[OH^-] + k_B[B] + k_A[A] + k_{A,B}[A][B] + k_{B,OH}[B][OH^-] \quad (1)$$

A comparison of the present data with those obtained for the rearrangement of **5b**[13b,17] and **5c**[5a] is of interest. On going from **5a** to **5b** and **5c,** a very large increase in the rate constant for the two base-catalyzed pathways is observed (calculated **5a**:**5b**:**5c** reactivity ratios at 298.15 K being ca. 1:220:23 000 and ca. 1:230:47 000 for k_{OH} and for k_B, respectively). This reflects the very different acidic character of protons, which strongly increases on going from the $-NH_2$ group in **5a** to the −NH−Ar and $-NH-Ar(NO_2)_2$ groups in **5b** and **5c**, respectively; thus, for example, at 293.15 K and pS^+ 12.0 $(k_{A,R})_{\mathbf{5a}}$:$(k_{A,R})_{\mathbf{5b}}$:$(k_{A,R})_{\mathbf{5c}}$ = 1:250:10 300. In contrast, in the uncatalyzed region a small reactivity difference between **5a** and **5b** has been observed [at pS^+ 6.0: $(k_{A,R})_{\mathbf{5b}}/(k_{A,R})_{\mathbf{5a}}$ ca. 2.5]. A comparison with **5c** is meaningless as this compound does not rearrange via an uncatalyzed pathway because of the very low nucleophilicity of its 2,4-dinitrophenylhydrazone nitrogen atom.[5a]

The values of the reactivity ratios obtained in the uncatalyzed and base-catalyzed regions can be explained by a complex interplay of two main factors: the nucleophilicity of the nitrogen atom and the acidity of the NH protons. These factors determine the substrate reactivity.[18,19] Let us compare first **5a** and **5b** along the uncatalyzed pathway. The high nucleophilicity of the nitrogen atom of **5a** would favor the new nitrogen−nitrogen bond formation, while the low acidity of the NH_2 protons should hamper the interaction with the solvent acting as a base. In **5b**, on the contrary, the lower nucleophilicity of nitrogen (compared to that of **5a**) would disfavor the new nitrogen−nitrogen bond formation, while the higher acidity of the NH proton should help the interaction with the solvent. This would explain the small reactivity difference experimentally observed on going from **5a** to **5b**. In contrast, in the base-catalyzed region, the acidity of the protons of the hydrazone moieties should become the dominant factor and overcome the importance of the nitrogen atom nucleophilicity, thus favoring **5b** and **5c** with respect to **5a**.

This picture agrees very well with the effects of the substituents that have been observed in the study of several *m*- and *p*-substituted arylhydrazones in both the uncatalyzed[20] and base-catalyzed range[21] and is strengthened by the observation that the kinetic isotopic effect is higher in the base-catalyzed (2.9) than in the uncatalyzed range (1.8).[17]

Finally, the analysis of the activation parameters for the rearrangement of **5a** (see Table 1) and **5b**[13b] has stressed an interesting trend. In the pS^+-independent range, the unfavorable enthalpy factor of **5a** is essentially balanced by the favorable entropy factor (lower overcrowding at the reaction center in **5a** with respect to **5b** and, consequently, a more efficient solvation and charge dispersion in the transition state). In contrast, in the pS^+-dependent range the entropy contribution is similar in the two cases and, therefore, *k* cannot balance the enthalpy contribution. Thus, **5b** becomes much more reactive than **5a**.

B. Computational Details. All the computations have been carried out with the Gaussian 98 series of programs.[22] The structures of the various critical points have been fully optimized with the gradient method and the nature of each critical point has been characterized by computing the harmonic vibrational frequencies. To choose a reliable computational approach, we have first investigated the structure of the 1,2,4-oxadiazole molecule (see Scheme 3) using the B3LYP[23] functional and

TABLE 3: Multiple Linear Regression Analysis[a] of Kinetic Data According to Eq 1 at 298 K

$10^5 k_u$ s^{-1}	$k_{OH} \pm s_{kOH}$ l mol^{-1} s^{-1}	$10^5(k_B \pm s_{kB})$ l mol^{-1} s^{-1}	$10^5(k_A \pm s_{kA})$ l mol^{-1} s^{-1}	$10^5(k_{A,B} \pm s_{kA,B})$ l mol^{-2} s^{-1}	$(k_{B,OH} \pm s_{kB,OH})$ l mol^{-2} s^{-1}	R
0.004 ± 0.004	0.017 ± 0.000	4.2 ± 0.2	0	0	0	1.000
0.016 ± 0.005	0.017 ± 0.000	4.5 ± 0.2	−0.9 ± 0.2	0	0	1.000
0.002 ± 0.005	0.017 ± 0.000	4.4 ± 0.3	0	0	−0.006 ± 0.007	1.000
0.008 ± 0.003	0.016 ± 0.000	5.1 ± 0.3	0	−61 ± 15	0	1.000

[a] s_{kOH}, s_{kB}, s_{kA}, $s_{kA,B}$, and $s_{kB,OH}$ are standard deviations of k_{OH}, k_B, k_A, $k_{A,B}$, and $k_{B,OH}$, respectively. *R*, multiple correlation coefficient. The number of points is 27 throughout.

SCHEME 3

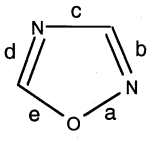

Geometrical parameters (ångstrom and degree):

	DZVP	6-311+G*	
a	1.411	1.407	(1.418)
b	1.309	1.301	(1.303)
c	1.380	1.376	(1.380)
d	1.300	1.294	--
e	1.341	1.334	--
<ab	102.9	102.8	--
<bc	115.4	115.4	--
<cd	101.3	101.3	--
<de	114.3	114.3	--
<ea	106.1	106.2	(114.2)

SCHEME 4

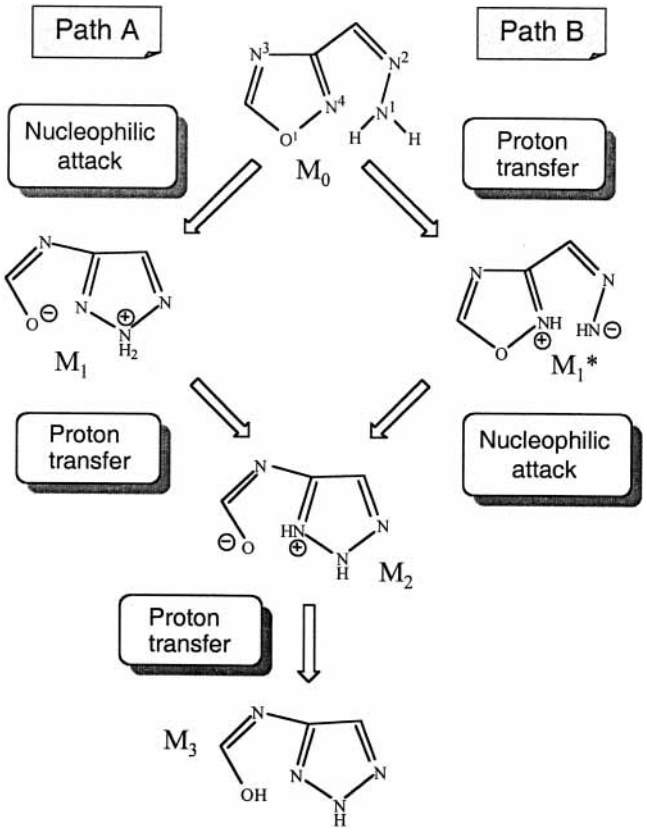

either the extended 6-311+G*[22] or the cheaper DZVP[24] basis set. DZVP is a local spin density (LSD) optimized basis set of double-ζ quality in the valence shell, which includes polarization functions. It is evident from the data reported in Scheme 3 that the two basis sets provide very similar results. Also, in both cases we have a quite satisfactory agreement with the experiment (see values in parentheses for the parameters **a**, **b**, **c,** and <**ea**). This computational evidence has prompted us to use the less expensive DZVP basis to investigate the **5d** → **6d** rearrangement.

The effect of the solvent environment has been evaluated using the continuum solvation model approach COSMO[25] as implemented in Gaussian 98.

C. Computational Results for the Rearrangement of 5d into 6d. The theoretical investigation has been carried out on a model system that emulates the reaction in the uncatalyzed region. In addition to a possible concerted path, we have considered two different, and equally plausible, multistep reaction pathways: path A and path B, schematically represented in Scheme 4. Along path A, the initial nucleophilic attack of nitrogen N^1 on nitrogen N^4 (formation of the intermediate M_1) is followed by two subsequent proton transfers: the first occurring from N^1 to N^4 (intermediate M_2) and the second from N^4 to the negative oxygen and leading to the final product M_3. Path B is characterized by an initial proton transfer from N^1 to N^4 (intermediate M_1*) followed by a nucleophilic attack which affords the intermediate M_2.

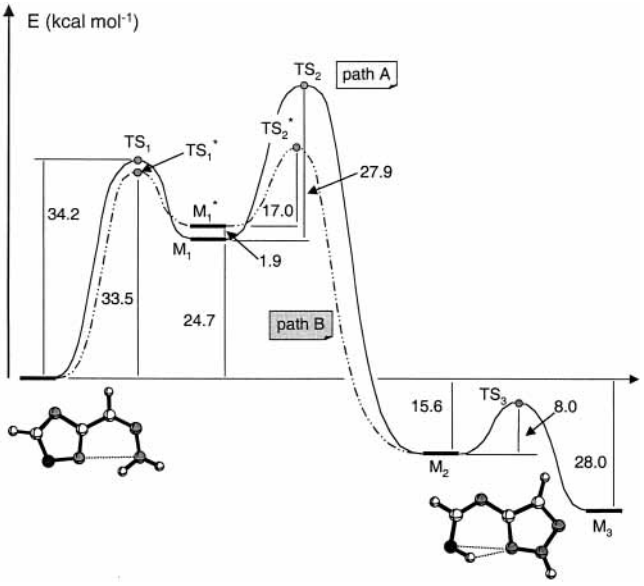

Figure 2. Model I. Energy profiles for path A and path B.

Three different model systems have been considered in our computations: Model I corresponding to the molecular system represented in Scheme 4 and Model II and Model III where one and two water molecules, respectively, have been explicitly considered. Furthermore, the COSMO continuum solvation model approach[25] has been used for Model III to evaluate the effects of the solvent environment. These effects can be particularly important in the present case where significant variations of the charge distribution are expected to occur along the reaction profile. Two different values for the dielectric constant ϵ_r have been used, that is, 78.30 (water) and 46.45 (dimethyl sulfoxide). The second value should emulate the effect of the dioxane/water mixture used in kinetic measurements. In the present section, the singlet potential energy surfaces (PES) associated with the ring-to-ring interconversion occurring in the three above model systems are discussed.

Model I. A schematic representation of the two reaction pathways (path A and path B) is given in Figure 2, while the structures of the corresponding critical points are represented in Figure 3 (path A) and Figure 4 (path B). Despite extensive search, no evidence for the existence of a concerted pathway has been found. A detailed description of the two paths is given in the following.

Path A. The nucleophilic attack of the nitrogen atom N^1 on the nitrogen N^4 (first step of the process) has a rather large activation barrier (34.2 kcal mol^{-1}, transition state TS_1). The attack leads to the intermediate M_1, which is 24.7 kcal mol^{-1} higher in energy than reactants. TS_1 is slightly reactant-like, as expected on the basis of the endothermic character of the reaction (see Figure 3). The significant structural changes involved in the nucleophilic attack (mainly a rotation around the N^2-N^1 bond to correctly orient the nitrogen lone pair, accompanied by a variation of the hybridization state from sp^2 to sp^3) can explain the high activation energy. A rotation by 90° of the terminal NH_2 group in M_0 provides a rotational barrier of 20.8 kcal mol^{-1}, which represents about 60% of the total barrier for the nucleophilic attack. On going from M_0 to M_1, significant variations of the various bond lengths are observed.

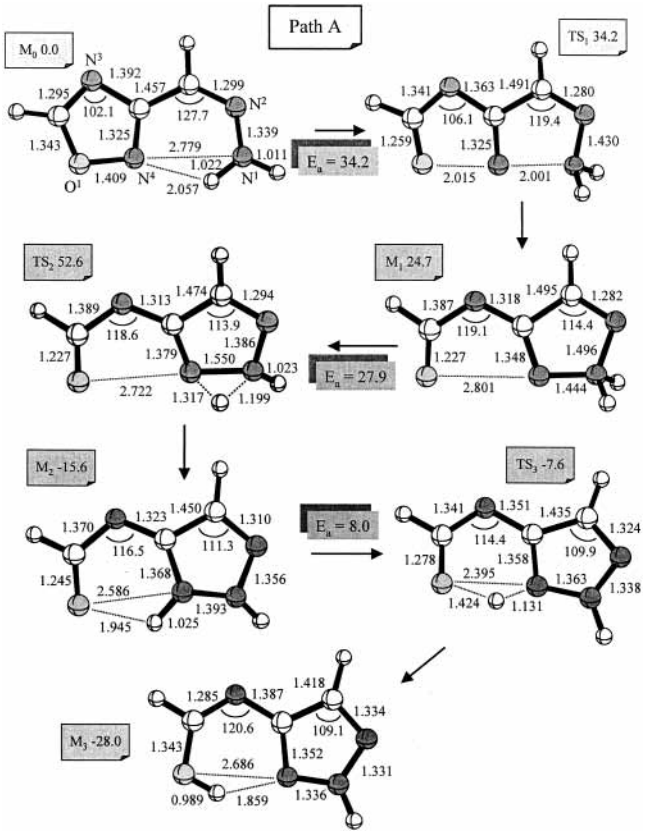

Figure 3. Schematic representation of the structures of the critical points located along path A for Model I (bond lengths are in angstroms and angles in degrees). The energy values (kcal mol^{-1}) relative to reactants (**M$_0$**) and the activation barriers E_a are reported.

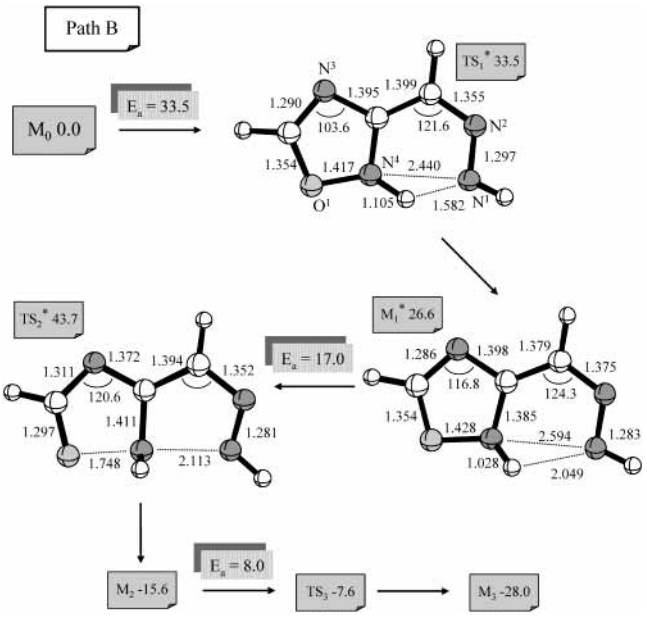

Figure 4. Schematic representation of the structures of the critical points located along path B for Model I (bond lengths are in angstroms and angles in degrees). The energy values (kcal mol^{-1}) relative to reactants (**M$_0$**) and the activation barriers E_a are reported.

In particular, the C−O^1 bond shows a significant increase of its double bond character (the length varies from 1.343 to 1.227 Å), while the two N^3−C bonds change from 1.295 and 1.392 Å to 1.387 and 1.318 Å, respectively. These structural changes are in agreement with the resonance picture reported in Scheme 5. A positive charge on the oxygen in structures II and III

SCHEME 5

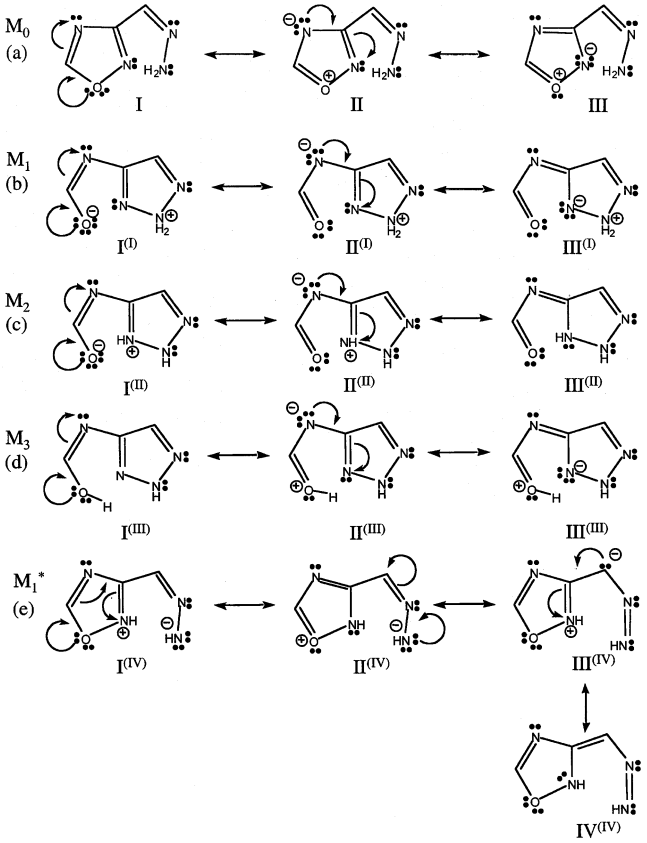

suggests that their contribution to M_0 is less significant than that of II$^{(I)}$ and III$^{(I)}$ to M_1.

A proton transfer from N^1 to N^4 leads to a much more stable intermediate M_2 (40.3 kcal mol^{-1} lower than M_1) by overcoming a barrier of 27.9 kcal mol^{-1}. In the corresponding transition state TS_2, the proton still significantly interacts with N^1 (the two N^1−H and N^4−H distances are 1.199 and 1.317 Å, respectively). The significant stabilization of M_2 can be explained by the strong aromatic character that characterizes a triazole ring[18,19] in contrast with the nonaromatic nature of M_1. This aromatic character makes M_2 more stable than the starting substrate. In this intermediate, the newly formed N^4−H bond (1.025 Å) has the suitable orientation to form a hydrogen bond with the oxygen atom (H···O^1 distance = 1.945 Å). As a consequence, we have a significant shortening of the N^4−O^1 distance (2.586 Å). The second proton transfer (transformation $M_2 \rightarrow TS_3 \rightarrow M_3$) requires a significantly lower activation barrier (only 8.0 kcal mol^{-1}). This low activation energy (when compared to that of the previous proton-transfer $M_1 \rightarrow TS_2 \rightarrow M_2$) can be easily understood. In TS_2, a re-hybridization of the atom N^1 is needed, while no re-hybridization process occurs in TS_3. Here, the proton easily migrates toward the properly oriented negative oxygen. In the product M_3, the C−O^1 bond has lost its double bond character (it is now 1.343 Å) in agreement with the resonance representation of Scheme 5 where the most important contributing structure to M_3 is I$^{(III)}$. The dominant contribution of I$^{(III)}$ also explains the shortening of the N_3–C bond (from 1.370 Å in M_2, where the dominant structure is III$^{(II)}$, to 1.285 Å in M_3). The strong hydrogen bond O^1−H···N^4 (H···N^4 distance = 1.859 Å) involving the transferred hydrogen provides a further stabilization to the final product.

Path B. The activation energy for the proton transfer occurring in the first step is again rather large (33.5 kcal mol^{-1}). This finding is in agreement with the formation of an unstable

intermediate species (M_1*) characterized by two separated charges (the formal charges on N^1 and N^4 in M_1* are −1 and +1, respectively). The geometrical features of M_1* are consistent with the resonance picture of Scheme 5, where the structures which mostly contribute are $I^{(IV)}$, $III^{(IV)}$, and $IV^{(IV)}$. Thus, the $C-O^1$ bond is mainly single in nature (1.354 Å) and the two N^3-C bonds are mainly double (1.286 Å) and single (1.398 Å), respectively. In particular, the shortening of the N^2-N^1 bond (1.283 Å) with respect to M_0 is due to the contributing structures $III^{(IV)}$ and $IV^{(IV)}$. A significant hydrogen bond ($N^{1}\cdots H-N$,[4] $H\cdots N^1$ = 2.049 Å) can be recognized in M_1*. The subsequent nucleophilic attack requires a much lower activation barrier (17.0 kcal mol^{-1}) than that found along path A. The lower energy barrier can be easily explained. No rotation around the N^1-N^2 bond is now necessary since the nitrogen lone pair (after proton transfer) has already the suitable orientation required for the attack. Thus, a contribution of about 20 kcal mol^{-1} (see previous section) can be subtracted from the barrier computed along path A (34.2 kcal mol^{-1}). This provides about 14 kcal mol^{-1}, rather close to that found here for the nucleophilic attack. Since this second step leads to the intermediate M_2, the third step of path B coincides with the corresponding step found along path A.

The previous discussion indicates the three-step reaction path B as the most convenient way to undergo the ring-to-ring interconversion. Thus, the simplest gas-phase model considered here does not support the experimentally based hypothesis that this rearrangement occurs in a concerted manner.

A further point should be stressed. It is well known that the DFT approach tends to underestimate the activation barriers for the S_N2 reactions[26] and provides values which are significantly lower than those obtained with the Hartree−Fock or correlated methods. To check this point, we have recomputed the two barriers for path A ($M_0 \rightarrow TS_1$) and path B ($M_0 \rightarrow TS_1^*$) at the HF level. The HF values are 42.3 and 41.6 kcal mol^{-1}, respectively. Even if they are significantly larger than DFT values, their difference remains constant (0.7 kcal mol^{-1}). This suggests that the possible underestimation of a few kcal mol^{-1} in the barriers will not affect the relative importance of the two paths.

Model II (One Water Molecule Included). The energy profiles for path A and path B are shown in Figure 5, while a detailed representation of the various critical points is given in Figures 6 and 7.

Path A. In the reactants, the water lies approximately in the molecular plane and forms two hydrogen bonds ($N^{4}\cdots H-O^2$ and $N^1-H\cdots O^2$) with the substrate. The first hydrogen bond causes a slight weakening of the N^4-O^1 bond (its length varies from 1.409 in Model I to 1.413 Å in Model II). At the same time, the negative charge on N^1 becomes more pronounced (from −0.58 in Model I to −0.64 here) and so does its nucleophilic character. As a consequence, the activation barrier for the nucleophilic attack decreases, being now 30.4 kcal mol^{-1}. Furthermore, the strength of the hydrogen bond $N^1-H\cdots O^2$ increases on passing from $M_0^{(1)}$ to the transition state $TS_1^{(1)}$ (the N^1-H and $H\cdots O^2$ distances change from 2.101 and 1.023 Å to 2.039 and 1.028 Å, respectively). This factor certainly stabilizes the transition state and concurs to lower the activation barrier.

It is interesting to examine the structure of the resulting intermediate $M_1^{(1)}$. Here, as found in $TS_1^{(1)}$, the water molecule lies above the molecular plane and simultaneously forms two rather strong hydrogen bonds: the $N^1-H\cdots O^2$ interaction ($H\cdots O^2$ = 1.824 Å) and the $O^{1}\cdots H-O^2$ interaction ($O^{1}\cdots H$ distance =

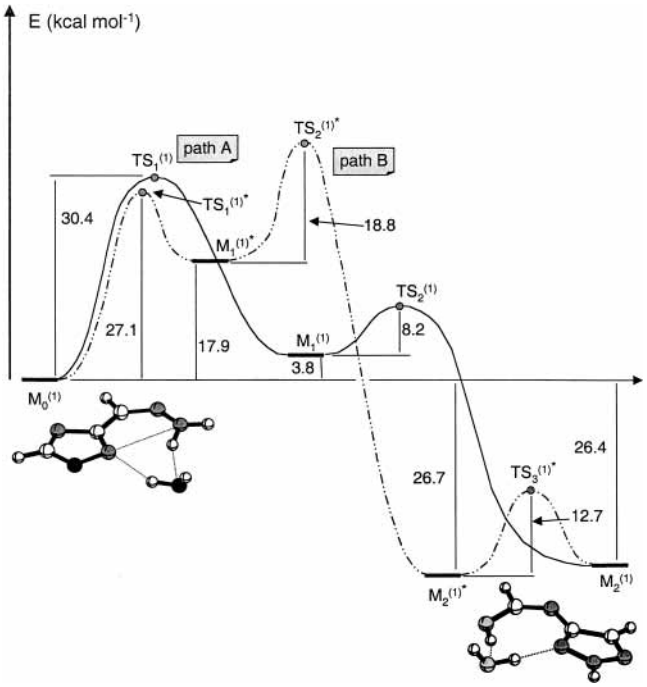

Figure 5. Model II. Energy profiles for path A and path B.

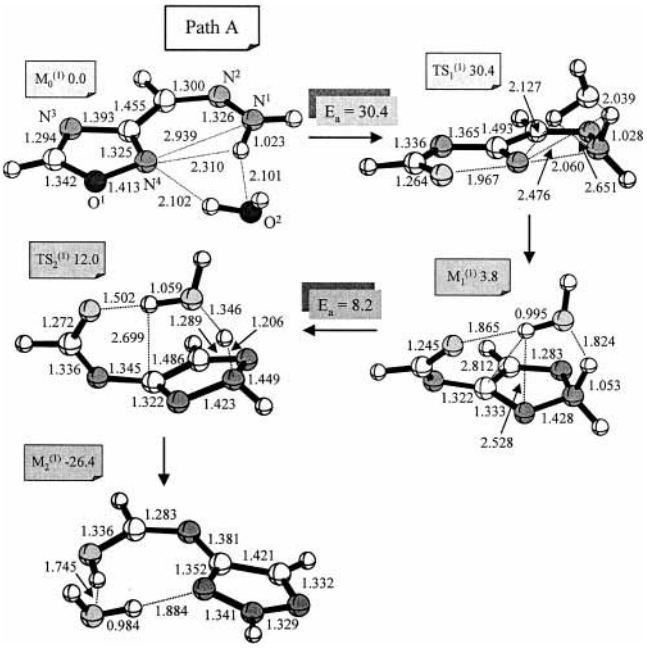

Figure 6. Schematic representation of the structures of the critical points located along path A for Model II (bond lengths are in angstroms and angles in degrees). The energy values (kcal mol^{-1}) relative to reactants ($\mathbf{M_0^{(1)}}$) and the activation barriers E_a are reported.

1.865 Å). An additional, but less strong, interaction involves the water hydrogen and the N^4 atom ($N^{4}\cdots H$ distance = 2.528 Å). The most interesting aspect is that, to enhance the $O^{1}\cdots H-O^2$ hydrogen bond, the molecule abandons the planar structure by rotating around the $C-N^3$ bond. This rotation places the $C-O^1$ bond in the right orientation to allow a simultaneous double proton transfer: one from N^1 to the water oxygen O^2 and the other from O^2 to the substrate oxygen O^1. This double proton transfer converts the three-step process of the gas-phase model into a two-step process and leads directly to the final product ($M_2^{(1)}$) by overcoming a barrier of only 8.2 kcal mol^{-1}. Thus this transformation, assisted by a water molecule, is a way

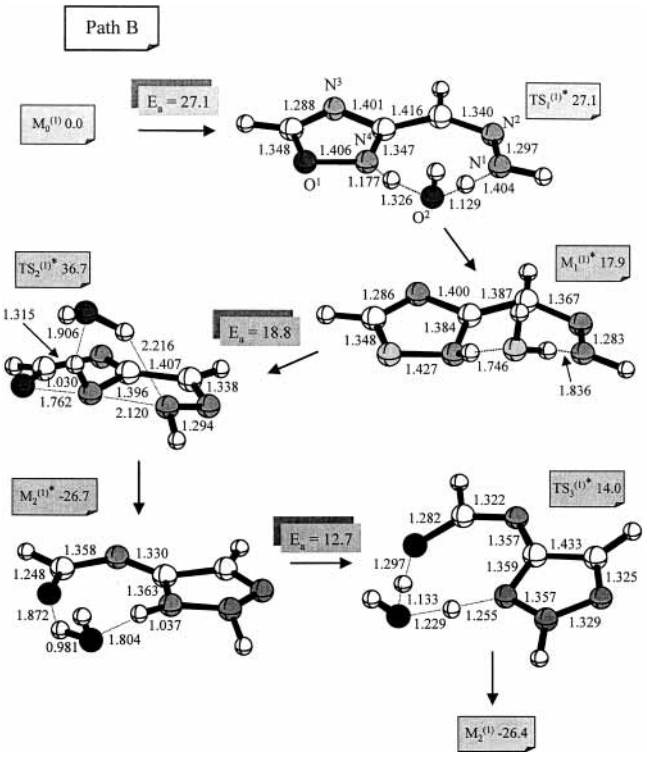

Figure 7. Schematic representation of the structures of the critical points located along path B for Model II (bond lengths are in angstroms and angles in degrees). The energy values (kcal mol^{-1}) relative to reactants ($\mathbf{M_0^{(1)}}$) and the activation barriers E_a are reported.

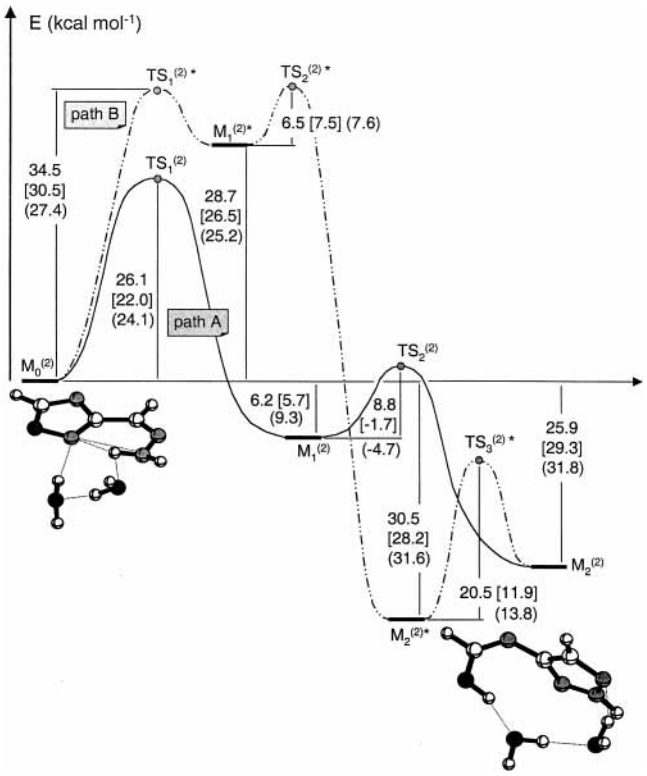

Figure 8. Model III. Energy profiles for path A and path B. Values in parentheses have been obtained by means of single-point computations with the COSMO method on the gas-phase optimized structures. Values in square brackets refer to dimethyl sulfoxide and values in round brackets to water.

to avoid the formation of the ammonium species observed in Model I (Step 2), which required a large activation energy (27.9 kcal mol^{-1}).

Path B. The presence of the water molecule has a less important effect on the energy profile of path B, which remains a three-step process. The first proton transfer (Step 1), which is assisted by a water molecule, has an activation barrier E_a of 27.1 kcal mol^{-1}. The decrease of E_a (of about 19%) with respect to Model I is probably due to the N^1−H···O^2 hydrogen bond, which determines a slight weakening of the N^1−H bond in $M_0^{(1)}$ (N^1−H distance = 1.023 Å). The barrier for the nucleophilic attack (18.8 kcal mol^{-1}) is again much lower than that found along path A and is similar to the path B value in Model I (17.0 kcal mol^{-1}). This is not surprising since in Model II, as found in Model I (path B), no rotation around the N^1−N^2 bond is needed. Finally, a barrier of 12.7 kcal mol^{-1} must be overcome to reach the final product $M_2^{(1)}$.

These results provide a mechanistic scenario that significantly differs from that found in Model I, where path B appears as the most likely reaction channel. In the presence of one solvent molecule acting as a base, even if the first step barrier is lower for path B (27.1 kcal mol^{-1}) than for path A (30.4 kcal mol^{-1}), the overcoming of the second barrier becomes much more difficult in the former case (18.8 kcal mol^{-1}) than in the latter (8.2 kcal mol^{-1}). Also, the barrier along path B for the reverse reaction $M_1^{(1)}* \rightarrow M_0^{(1)}$ is only 9.2 kcal mol^{-1}, which is very similar to that of the final transformation along path A. These results indicate now that path A is the favored channel to afford the ring-to-ring interconversion.

Model III (Two Water Molecules Included). To elucidate the effect of one additional solvent molecule on the reaction surface, path A and path B have been reinvestigated in the presence of two water molecules. The corresponding energy profiles are reported in Figure 8 and the structures of the critical points are represented in Figure 9 (path A) and 10 (path B).

Path A. In the reactants, the two water molecules are one above the molecular plane and the other on the opposite side and form a complex net of hydrogen bonds. The nucleophilic attack requires now an energy barrier of 26.1 kcal mol^{-1}. This value, though still large, is lower than that found in Model II. The decrease of E_a can be ascribed to the increase in strength of the three hydrogen bonds O^2−H···N^4, O^{2}···H−O^3, and O^3···H−N^1 on passing from $M_0^{(2)}$ to the transition state $TS_1^{(2)}$ (the N^4···H, O^2···H, and O^3···H distances change from 2.060, 1.871, and 2.553 Å in $M_0^{(2)}$ to 1.984, 1.786, and 1.842 Å in $TS_1^{(2)}$, respectively). Also, an additional interaction O^2−H···O^1 (H···O^1 = 2.543 Å) can be recognized in $TS_1^{(2)}$. In the resulting intermediate $M_1^{(2)}$, the two water molecules are both above the molecular plane and form a chain of three hydrogen bonds connecting N^1 to the substrate negative oxygen. These hydrogen bonds are rather strong (O^1···H, O^2···H, and O^3···H are 1.760, 1.661, and 1.605 Å, respectively) and contribute to stabilize $M_1^{(2)}$, 6.2 kcal mol^{-1} lower than reactants. The position of the two water molecules in $M_1^{(2)}$ represents the best arrangement for a triple proton transfer from N^1 to the terminal oxygen O^1 to afford the final product $M_2^{(2)}$. The activation energy required for this step (8.8 kcal mol^{-1}) is close to that determined for Model II (8.2 kcal mol^{-1}). In conclusion, the presence of two water molecules does not modify substantially the main features of path A, which remains a two-step process with the rate-determining step represented by the nucleophilic attack.

Path B. In the presence of two water molecules, this path becomes even more unlikely than in Model II, since a large barrier (34.5 kcal mol^{-1}) characterizes now the first step (proton transfer from N^1 to N^4). The magnitude of this barrier is probably caused by the loss of one hydrogen bond

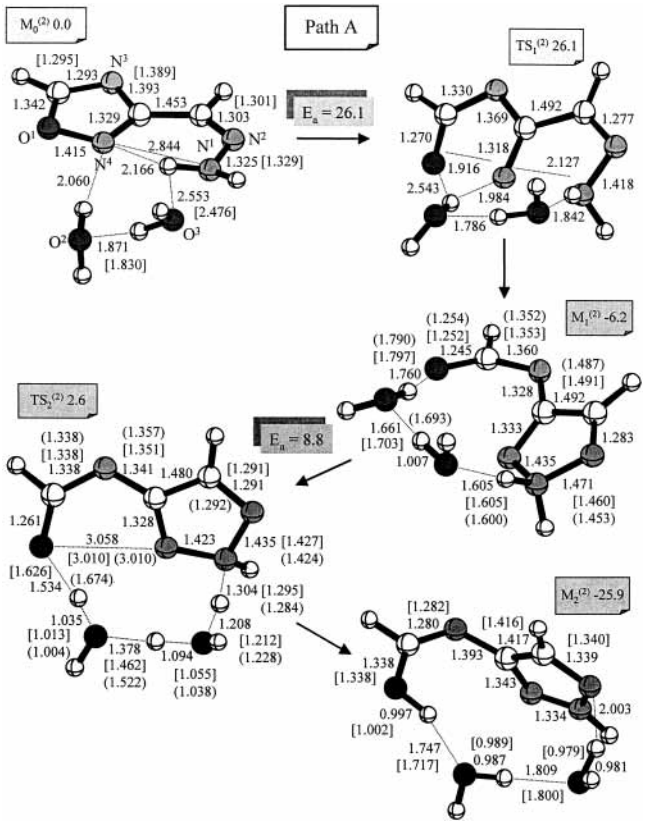

Figure 9. Schematic representation of the structures of the critical points located along path A for Model III (bond lengths are in angstroms and angles in degrees). The energy values (kcal mol^{-1}) relative to reactants ($\mathbf{M_0^{(2)}}$) and the activation barriers E_a are reported. The values in parentheses have been obtained after geometry optimization in the presence of solvent effects. Values in square brackets refer to dimethyl sulfoxide and values in round brackets to water.

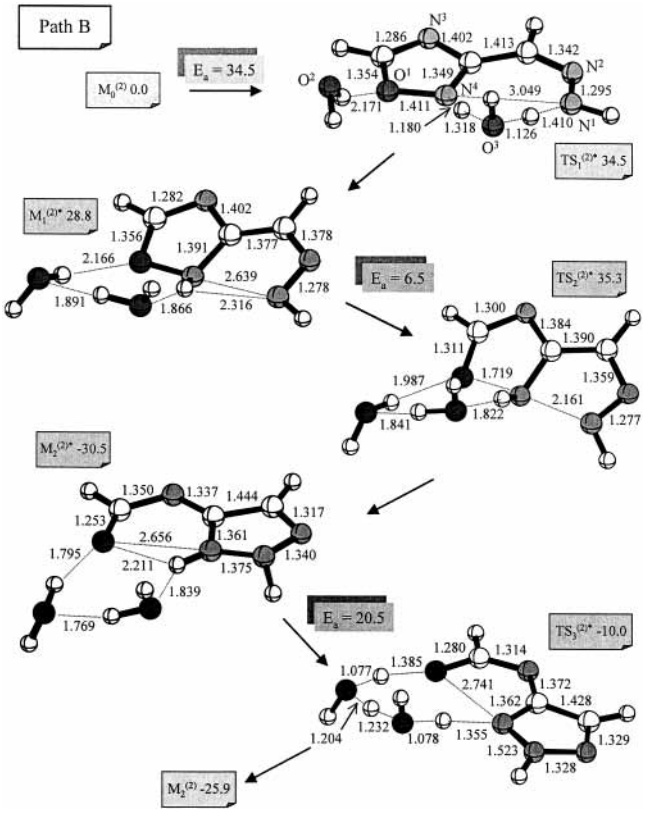

Figure 10. Schematic representation of the structures of the critical points located along path B for Model III (bond lengths are in angstroms and angles in degrees). The energy values (kcal mol^{-1}) relative to reactants ($\mathbf{M_0^{(2)}}$) and the activation barriers E_a are reported.

($N^{4}\cdots H-O^{2}$) in the transformation $M_0^{(2)} \rightarrow TS_1^{(2)}$*. The relative energy of the resulting intermediate $M_1^{(2)}$* increases with respect to Model II (it is now 28.7 kcal mol^{-1} higher than reactants). This can be again explained by the weakening of the hydrogen bond network occurring in $M_1^{(2)}$*. A low barrier (6.5 kcal mol^{-1}) is needed by the nucleophilic attack to afford the highly stable intermediate $M_2^{(2)}$*, 30.5 kcal mol^{-1} lower than $M_0^{(2)}$. The third step, which has a rather large activation energy (20.5 kcal mol^{-1}), is again a triple proton transfer from N^4 to the substrate negative oxygen O^1. The comparison between the two reaction channels clearly points to the two-step path A as the most likely way to carry out the ring-to-ring interconversion. Thus, even in the presence of two solvent molecules, that we have demonstrated to be directly involved in the reaction, there is no evidence for a concerted pathway in contrast to the experimental indications.

D. The Effect of the Solvent Environment. The effect of the solvent on the energy profiles has been evaluated for Model III for both path A and path B by means of single-point computations on the previously described structures (gas-phase structures). The relative energies and the energy barriers obtained in the presence of solvent effects are reported in Figure 8 in square (dimethyl sulfoxide) and round (water) brackets.

The solvent effects do not affect significantly path B, which remains a three-step process where the two most important barriers correspond to the first and third step (proton transfers). In the former case the barrier decreases from 34.5 to 30.5 (dimethyl sulfoxide) and 27.4 (water) kcal mol^{-1} and in the latter from 20.5 to 11.9 and 13.8 kcal mol^{-1}, respectively. The second step is still characterized by a small barrier (7.5 and 7.6 kcal mol^{-1} in dimethyl sulfoxide and water, respectively). More interesting are the results obtained for path A that suggest a novel mechanistic scenario. While the first barrier slightly decreases becoming 22.0 (dimethyl sulfoxide) and 24.1 kcal mol^{-1} (water), the effect of the solvent environment on the energy of $TS_2^{(2)}$ is more dramatic. This transition state becomes more stable than the starting intermediate $M_1^{(2)}$ (1.7 kcal mol^{-1} in dimethyl sulfoxide and 4.7 kcal mol^{-1} in water) suggesting the existence of a concerted pathway. Thus, these computational evidences indicate that in the real experimental conditions the preferred pathway A would correspond to a concerted asynchronous (or two-phase) process. In a process of this type, we have only one kinetic step (only one energy barrier can be detected), but the nucleophilic attack and the proton transfer occur in two subsequent phases of the process and not simultaneously. The corresponding energy profile is characterized, in general, by a primary maximum, which determines the activation energy. In some cases, it is possible to detect a secondary (very small) maximum which tends to disappear, thus originating an inflection point.

To validate the results obtained by means of single-point computations on the gas-phase structures and to discard the hypothesis of a computational shortcoming due to the lack of geometry optimization, we have re-optimized the structure of some critical points along the preferred pathway A ($M_0^{(2)}$, $M_1^{(2)}$, $TS_2^{(2)}$, and $M_2^{(2)}$) in the presence of the solvent effects. The new geometrical parameters are reported in Figure 9 in square (dimethyl sulfoxide) and round (water) brackets. It is evident that the solvent effects do not substantially affect them. The most interesting results concern the two critical points $M_1^{(2)}$ and $TS_2^{(2)}$. Even if these two points can still be located on the potential surface, a considerable decrease of the $M_1^{(2)} \rightarrow TS_2^{(2)}$

activation barrier is observed. This barrier becomes 2.5 kcal mol^{-1} in dimethyl sulfoxide and further decreases in water (1.5 kcal mol^{-1}). Thus, these results are consistent with the single-point computations previously discussed even if those computations clearly overestimate the energy lowering of $TS_2^{(2)}$. Anyhow, both sets of data (single-point computations and geometry re-optimization) definitely indicate that the solvent makes the $M_1^{(2)} \rightarrow TS_2^{(2)}$ barrier negligible and the two-step reaction path A becomes more and more similar to a concerted asynchronous pathway.

Conclusions

In this paper, we have carried out a combined kinetic and theoretical study of the monocyclic rearrangements of heterocycles (MRH), a ring-to-ring interconversion process of wide synthetic interest. The experimental investigation has been carried out on the rearrangement of the *Z*-hydrazone of 3-benzoyl-5-phenyl-1,2,4-oxadiazole **5a** into the 1,2,3-triazole **6a** in dioxane/water in the pS^+ range $5.5_5-13.9$. The possible paths for this reaction in the uncatalyzed range have been studied at the DFT level on a model system formed by the *Z*-hydrazone of 3-formyl-1,2,4-oxadiazole (**5d**). Either one or two water molecules have been explicitly considered to clarify the active role of solvent molecules. The effect of the solvent environment has been estimated with the COSMO continuum model approach. Our results provide an exhaustive mechanistic picture for these processes and definitely confirm the hypothesis proposed on the basis of previous kinetic studies.[13b] The most important points can be summarized as follows.

(i) The kinetic data of the present study and their comparison to those obtained in previous work for the *Z*-phenylhydrazone and the *Z*-2,4-dinitrophenylhydrazone of 3-benzoyl-5-phenyl-1,2,4-oxadiazole suggest a concerted process where the substrate reactivity is the result of the interplay of two factors, that is, the nucleophilicity of the nitrogen atom and the acidity of the nitrogen-bonded protons. These two factors act in opposite directions and determine the magnitude of the activation barrier.

(ii) Two different multistep pathways have been recognized at the theoretical level. In one case (path A), the first event is the nucleophilic attack followed by a multiple proton transfer. In the other case (path B), the nucleophilic attack occurs after an initial deprotonation of the nucleophile and a second proton transfer affords the final product.

(iii) When the effect of the solvent environment is not taken into account, no computational evidence for a concerted pathway has been found. The preferred reaction pathway is the two-step path A where the rate-determining step has an activation barrier of 26.1 kcal mol^{-1}.

(iv) The effect of the solvent is crucial in determining the energy profile of the favored path A. While the barrier of the first step (rate-determining) only slightly decreases (from 26.1 to 24.1 in water and 22.0 kcal mol^{-1} in dimethyl sulfoxide), the second step tends to disappear. This suggests that in the real experimental conditions the reaction should proceed along a concerted highly asynchronous path (two-phase process) where the nucleophilic attack and the proton transfer occur in the same kinetic step but are not simultaneous. The estimate of the activation barrier (in the range 24.1−22.0 kcal mol^{-1}) is in good agreement with the experimental activation enthalpy (25.1 kcal mol^{-1}).

Experimental Section

General Methods. ^{1}H NMR spectra were recorded in the Fourier transform mode at 21.0 ± 0.5 °C in DMSO-d_6. Chemical shifts (δ) are in ppm from tetramethylsilane. Mass spectra were recorded at chemical ionization (CI) on a VG70 70E apparatus.

***Z*-(5-Phenyl-1,2,4-oxadiazol-3-yl)(phenyl)methanone *N*-Hydrazone (5a)**. Hydrazine hydrate (85%, 0.3 g, 5.1 mmol) dissolved in ethanol (3 mL) was dropwise added under stirring to a solution of 3-benzoyl-5-phenyl-1,2,4-oxadiazole (1 g, 4 mmol) in ethanol (15 mL). The mixture was heated 4 h in a water bath and the resulting solution evaporated at reduced pressure. The obtained residue by chromatography (ethyl acetate/petroleum ether 40−60 °C = 1:5, v/v) gave, in order of elution, the *Z*- and the *E*-isomers. *Z*-**5a** 0.45 g 43%. Mp 112 °C from ethanol. NMR δ_H: 7.24−7.43 (m, 3H, ArH); 7.58−7.80 (m, 5H, ArH); 8.19 (m, 2H, *ortho* ArH); 8.49 (s, 2H, NH_2). HRMS: 264.100784, $C_{15}H_{12}N_4O$ requires 264.101111. UV−vis spectrum in dioxane/water 1:1 (v:v) λ_{max} 258 nm, log ϵ_{max} 4.41. *E*-**5a** 0.30 g 28%. Mp 145 °C from ethanol. NMR δ_H: 7.41 (s, 2H, NH_2); 7.34−7.75 (m, 8H, ArH); 8.10 (m, 2H, *ortho*, ArH); 8.49 (s, 2H, NH_2). HRMS: 264.100981, $C_{15}H_{12}N_4O$ requires 264.101111.

The used synthetic procedure recalls that used by Ruccia and Spinelli, who reported physical data for the not-separated mixture of the two geometric isomers.[27]

4-Benzoylamino-5-phenyl-2*H*-1,2,3-triazole (6a). Compound **6a** was prepared and purified according to a reported method.[27] Mp 191 °C (lit.[27] 190) from ethanol. HRMS: 264.100529, $C_{15}H_{12}N_4O$ requires 264.101111. UV−vis spectrum in dioxane/water 1:1 (v:v) λ_{max} 242 nm, log ϵ_{max} 4.23.

pS^+ Scale Definition and Kinetic Measurements. Water and dioxane were purified according to literature methods.[28] Details on the pS^+ scale have already been reported.[13a] The kinetics were followed spectrophotometrically, as previously described,[13b] by measuring the disappearance of **5a** at 280 nm (where the observed optical-density difference between starting and final products is largest) by using a UV−vis spectrophotometer Zeiss PMQII (pS^+ $5.5_5-13.9$). The rate constants are accurate within ±3%. Apparent first-order kinetic constants [$(k_{A,R})_{\mathbf{5a}}$] calculated at 293.15 K are reported in Table 1. The concentrations used were about 8.5×10^{-5} M.

The values $(k_{A,R})_{\mathbf{5a}}$ for general base catalysis determination at different buffer concentrations have been calculated at 298.15 K from thermodynamic parameters in the pS^+ range 10.9−12.5 (Table 2) and managed as previously described.[17]

Acknowledgment. We thank MURST (Ministero dell'Università e della Ricerca Scientifica e Tecnologica, Roma) Roma, PRIN-2002 and CNR (Consiglio Nazionale delle Ricerca, Roma) for financial support. Investigations were supported by the Universities of Bologna and Palermo (funds for selected research topics).

Supporting Information Available: Total energies and Cartesian coordinates of minima and transition states. This material is available free of charge via the Internet at http://pubs.acs.org.

References and Notes

(1) (a) Boulton, A. J. *Lectures in Heterocyclic Chemistry*; HeteroCorporation: Provo, UT, 1973. (b) Boulton, A. J.; Katritzky, A. R.; Majid-Hamid, A. *J. Chem. Soc. C* **1967**, 2005−2007. (c) Katritzky, A. R.; Gordev, M. F. *Heterocycles* **1993**, *35*, 483−518. (d) Ghosh, B. P. *J. Chem. Soc. B* **1968**, 334−338. (e) Buncel, E.; Chuaqui-Offermanns, N.; Norris, A. *Can. J. Chem.* **1979**, *57*, 2512−2515.

(2) (a) Boulton, A. J.; Ghosh, P. B.; Katritzky, A. R. *J. Chem. Soc. B* **1966**, 1004−1010. (b) Boulton, A. J.; Ghosh, P. B.; Katritzky, A. R. *J. Chem. Soc. B* **1966**, 1011−1015.

(3) (a) Eckert, F.; Rauhut, G. *J. Am. Chem. Soc.* **1998**, *120*, 13478−13484. (b) Rauhut, G.; Eckert, F. *Sci. Progress* **1999**, *82*, 209−231. (c) Eckert, F.; Rauhut, G.; Katritzky, A. R.; Steel, J. P. *J. Am. Chem. Soc.*

1999, *121*, 6700−6711. (d) Rauhut, G. *J. Org. Chem.* **2001**, *66*, 5444−5448 and references therein.

(4) (a) Van der Plas, H. C. *Ring Transformations of Heterocycles*; Academic Press: London, 1973; Vols 1 and 2. (b) L'abbé, G. *J. Heterocycl. Chem.* **1984**, *21*, 627−638. (c) Ruccia, M.; Vivona, N.; Spinelli, D. *Adv. Heterocycl. Chem.* **1981**, *29*, 141−169. (d) Vivona, N.; Buscemi, S.; Frenna, V.; Cusmano, G. *Adv. Heterocycl. Chem.* **1993**, *56*, 49−154. (e) Korbonits, D.; Bakò, E. M.; Horváth, K. *J. Chem. Res., Synop*. **1979**, 64−65; *J. Chem. Res., Miniprint* **1979**, 801−875.

(5) (a) Cosimelli, B.; Guernelli, S.; Spinelli, D.; Buscemi, S.; Frenna, V.; Macaluso, G. *J. Org. Chem.* **2001**, *66*, 6124−6129. (b) Cosimelli, B.; Frenna, V.; Guernelli, S.; Lanza, C. Z.; Macaluso, G.; Petrillo, G.; Spinelli, D. *J. Org. Chem.* **2002**, *67*, 8010−8018. (c) Guernelli, S.; Laganà, M. F.; Spinelli, D.; Lo Meo, P.; Noto, R.; Riela, S. *J. Org. Chem.* **2002**, *67*, 2948−2953. (d) Guernelli, S.; Noto, R.; Sbrizziolo, C.; Spinelli, D.; Turco Liveri, M. L. *J. Colloid Interface Sci*. **2001**, *239*, 217−221. (e) Buscemi, S.; Vivona, N. *Heterocycles* **1994**, *38*, 2423−2432. (f) Buscemi, S.; Pace, A.; Frenna, V.; Vivona, N. *Heterocycles* **2002**, *57*, 811−823.

(6) Harsányi, K. *J. Heterocycl. Chem.* **1973**, *10*, 957−961.

(7) (a) Korbonits, D.; Kanzel-Svoboda, I.; Horváth, K. *J. Chem. Soc., Perkin Trans. 1* **1982**, 759−766. (b) Horváth, K.; Korbonits, D.; Náray-Szabó, G.; Simon, K. *THEOCHEM* **1986**, *136*, 215−227.

(8) Frenna, V.; Spinelli, D.; Consiglio, G. *J. Chem. Soc., Perkin Trans. 2* **1990**, 1289−1295.

(9) (a) Frenna, V.; Vivona, N.; Consiglio, G.; Spinelli, D.; Mezzina, E. *J. Chem. Soc., Perkin Trans. 2* **1993**, 1339−1343. (b) Frenna, V.; Macaluso, G.; Vivona, N.; Spinelli, D., Consiglio, G.; Mezzina, E. *Tetrahedron* **1994**, *50*, 7315−7326.

(10) (a) Vivona, N.; Cusmano, G.; Ruccia, M.; Spinelli, D. *J. Heterocycl. Chem.* **1975**, *12*, 985−988. (b) Vivona, N.; Ruccia, M.; Cusmano, G.; Marino, M. L.; Spinelli, D. *J. Heterocycl. Chem.* **1975**, *12*, 1327−1328. (c) La Manna, G.; Buscemi, S.; Frenna, V.; Vivona, N.; Spinelli, D. *Heterocycles* **1991**, *32*, 1547−1557. (d) Buscemi, S.; Frenna, V.; Vivona, N.; Petrillo, G.; Spinelli, D. *Tetrahedron* **1995**, *51*, 5133−5142. (e) La Manna, G.; Buscemi, S.; Vivona, N. *J. Mol. Struct. (THEOCHEM)* **1998**, *452*, 67−74. (f) Buscemi, S.; Frenna, V.; Pace, A.; Vivona, N.; Cosimelli, B.; Spinelli, D. *Eur. J. Org. Chem.* **2002**, 1417−1423. (g) Andrianov, V. G.; Makushenkov, S. V.; Eremeev, A. V. *Mendeleev Commun.* **1992**, 129−130.

(11) The uncatalized pathway has been evidenced in protic solvent (dioxane/water and methanol) with high permittivity and basicity (Reichardt, C. *Solvents and Solvent Effects in Organic Chemistry*, 3rd ed.; Wiley-VCH: Weinheim, Germany, 2003) as well as in dipolar aprotic solvents (acetonitrile); this pathway has not been observed in solvent such as benzene, while in dioxane and ethyl acetate (Frenna, V.; Vivona, N.; Consiglio, G.; Spinelli, D. *J. Chem. Soc., Perkin Trans. 2* **1983**, 1199−1202) very low kinetic constants have been measured ($(2-3) \times 10^{-7}$ s^{-1}). These results well fit the observation that, e.g., hydrazones are stable compounds in the solid state.

(12) (a) Frenna, V.; Vivona, N.; Macaluso, G.; Spinelli, D.; Consiglio, G. *J. Chem. Soc., Perkin Trans. 2* **1987**, 537−540. (b) Frenna, V.; Buscemi, S.; Arnone, C. *J. Chem. Soc., Perkin Trans. 2* **1988**, 1683−1686. (c) Ruccia, M.; Vivona, N.; Cusmano, G.; Macaluso, G. *J. Chem. Soc., Perkin Trans. 1* **1977**, 589−591. (d) Vivona, N.; Cusmano, G.; Macaluso, G. *J. Chem. Soc., Perkin Trans. 1* **1977**, 1616−1619.

(13) (a) An operational pH scale, pS^+ (Bates, R. G. In *Solute−Solvent Interactions*; Coetze, J. F., Ritchie, C. D., Eds.; Marcel Dekker: New York, 1969; p 46), was established in aqueous dioxane by employing the pK_a values of acids determined by interpolation from the data reported by Harned and Owen (Harned, H. S.; Owen, B. B. *The Physical Chemistry of Electrolytic Solution*, 3rd ed.; ACS Monograph No. 137; Reinhold: New York, 1970; pp 716, 755). For dioxane−water (1:1, v/v) the meter reading after calibration against buffers was not significantly different from pS^+, requiring a correction of only +0.16. (b) Spinelli, D.; Corrao, A.; Frenna, V.; Vivona, N.; Ruccia, M.; Cusmano, G. *J. Heterocycl. Chem.* **1976**, *13*, 357−360.

(14) At lower pS^+ values, the acidic hydrolysis of **5a** significantly competes with its rearrangement; this behavior duplicates that observed in the instance of **5b**[13b] and **5c**[5a] at p$S^+ < 3.5$. It is well known that hydrazones, more basic than arylhydrazones, are hydrolyzed at lower proton concentrations.

(15) (a) Laidler, K. J. *Chemical Kinetics*; McGraw-Hill: London, 1965; p 457. (b) Laidler, K. J.; Bunting, P. S. *The Chemical Kinetics of Enzyme Action*; Clarendon Press: Oxford, 1973; p 60. (c) This outcome well fits Hammett's criterion (Hammett, L. P. *Physical Organic Chemistry*, 2nd ed.; McGraw-Hill: New York, 1970; pp 322−323) for the identification of the kind of catalysis.

(16) (a) Ritchie, C. D. *Physical Organic Chemistry, The Fundamental Concepts*; M. Dekker: New York, 1975; Chapter 7. (b) Exner, O. *Correlation Analysis of Chemical Data*; Plenum Press: New York and London, 1988; Chapter 7.4. (c) Williams, A. *Concerted Organic and Bio-organic Mechanisms*; CRC Press: Boca Baton, FL, 2000. (d) Carey, F. A.; Sundberg, R. J. *Advanced Organic Chemistry*; Kluwer Academic/Plenum Publishers: New York, 2000; Chapter 4.8.

(17) Frenna, V.; Vivona, N.; Consiglio, G.; Corrao, A.; Spinelli, D. *J. Chem. Soc., Perkin Trans. 2* **1981**, 1325−1328.

(18) (a) Bird, C. W. *Tetrahedron* **1985**, *41*, 1409−1414. (b) Bird, C. W. *Tetrahedron* **1992**, *48*, 335−340. (c) Katritzky, A. R.; Jug, K.; Oniciu, D. C. *Chem. Rev.* **2001**, *110*, 1421−1449. (d) Katritzky, A. R.; Barczynsky, P.; Musumarra, G.; Pisano, D.; Szafran, M. *J. Am. Chem. Soc.* **1989**, *111*, 7−15.

(19) (a) Katritzky, A. R.; Pozharskii, A. F. *Handbook of Heterocyclic Chemistry*, 2nd ed.; Pergamon: Oxford, U.K., 2000; pp 101−102. (b) Bean, P. G. *J. Org. Chem.* **1988**, *53*, 2497−2506.

(20) Spinelli, D.; Frenna, V.; Corrao, A.; Vivona, N. *J. Chem. Soc., Perkin Trans. 2* **1978**, 19−22.

(21) Frenna, V.; Vivona, N.; Corrao, A.; Consiglio, G.; Spinelli D. *J. Chem. Res. Synop.* **1981**, 308−309; *Chem. Res. Miniprint* **1981**, 3550−3578.

(22) *Gaussian 98*, Revision A.6; Frisch, M. J.; Trucks, G. W.; Schlegel, H. B.; Scuseria, E. G.; Robb, M. A.; Cheeseman, J. R.; Zakrzewski, V. G.; Montgomery, J. A.; Stratmann, R. E.; Burant, J. C.; Dapprich, S.; Millam, J. M.; Daniels, A. D.; Kudin, K. N.; Strain, M. C.; Farkas, O.; Tomasi, J.; Barone, V.; Cossi, M.; Cammi, R.; Mennucci, B.; Pomelli, C.; Adamo, C.; Clifford, S.; Ochterski, J.; Petersson, G. A.; Cui, Q.; Morokuma, K.; Malik, D. K.; Rabuck, A. D.; Raghavachari, K.; Foresman, J. B.; Cioslowski, J.; Ortiz, J. V.; Stefanov, B. B.; Liu, G.; Liashenko, A.; Piskorz, P.; Kamaromi, I.; Gomperts, R.; Martin, R. L.; Fox, D. J.; Keith, T.; Al-Laham, M. A.; Peng, C. Y.; Nanayakkara, A.; Gonzalez, C.; Challacombe, M.; Gill, P. M. W.; Johnson, B. G.; Chen, W.; Wong, M. W.; Andres, J. L.; Gonzalez, C.; Head-Gordon, M.; Replogle, E. S.; J. A. Pople Gaussian, Inc.: Pittsburgh, PA.

(23) Becke, A. D. *J. Chem. Phys.* **1993**, *98*, 5648.

(24) Godbout, N.; Salahub, D. R.; Andzelm, J.; Wimmer, E. *Can. J. Chem.* **1992**, *70*, 560. *UniChem DGauss*, Version 2.3.1; Cray Research, Inc., Mendota Heights, MN 55120, 1994.

(25) Klamnt, A. *J. Phys. Chem.* **1995**, *99*, 2224; **1996**, *100*, 3349.

(26) Deng, L.; Branchadell, V.; Ziegler, T. *J. Am. Chem. Soc.* **1994**, *116*, 10645−10656.

(27) Ruccia, M.; Spinelli, D. *Gazzetta* **1959**, *89*, 1654−1669.

(28) Weissberger, A. *Technique of Organic Chemistry*, 2nd ed.; Interscience: New York, **1963**; Vol. 7.